New Approximation Method for High Order Impedance Boundary Condition with Surface Integral Equations for the Scattering Problem

Christian Daveau, Soumaya Oueslati, Molka Kacem

New Approximation Method for High Order Impedance Boundary Condition with Surface Integral Equations for the Scattering Problem

Christian Daveau [*], Soumaya Oueslati [†], Molka Kacem[‡]

October 24, 2023

Abstract

In this paper, we propose a new method to approximate operators resulted from solving the scattering Problem in electromagnetism by dielectrically coated conducting bodies, using integral equations and high order impedance boundary condition. We introduce the variational Problem and we prove that it is well-posed, we present the new theoretical approach and highlight its potential through numerical experiments.

Keywords: scattering problem, high order boundary condition, existence and uniqueness, Lax-Milgram, integral operators, radar cross section.

[*]CY Cergy Paris University, e-mail: christian.daveau@cyu.fr
[†]CY Cergy Paris University, e-mail: soumaya.oueslati1@cyu.fr
[‡]CY Cergy Paris University, e-mail: molka.kacem@cyu.fr

1 Introduction

The problem of electromagnetic scattering by conducting objects (PEC) coated with dielectric materials has been of considerable and growing interest due to its significance in radar prediction of targets, stealth technology, geophysics, and antennas ([1],[2],[3]). This significance is also fortified by the need to enhance the computational efficiency of the existing techniques. The exact solution is only available for special class of geometries such as the coated conducting sphere. For an arbitrary cross-section, one has to resort to a numerical technique which guarantees the accuracy ([4],[5],[6],[7]) and efficiency of the solution such as the Poggio-Miller formulation- Chang-Harrington-Wu-Tsai (PMCHWT) reference ([8],[9],[10]).

There are several numerical methods to solve the electromagnetic scattering problem (finite-difference [11], finite-volume [12], method of moments MoM [13],etc.), we are particularly interested in the method of moments.

The volumic surface integral equation (VSIE) ([14],[15],[16],[17]) and the surface integral equation (SIE) ([13], [4],[1],[18],[19],[20],[21],[22]) in conjunction with the method of moments (MoM) are the most powerful techniques to solve this problem numerically, each one has its advantages and its disadvantages depending on the considered problem ([23],[24],[25]).

The SIE is considered more advantageous than VSIE for homogeneous coating materials, because, the surface equivalence principle is used to model each homogeneous region with unknown equivalent currents placed on the surface of this region, compared to VSIE, where the unknown equivalent currents are distributed throughout the layer volume.

Different SIE formulations have been devised to solve the electromagnetic scattering problem by a coated conductive object. Among these formulations are the SIE formulation using the electric field integral equation (EFIE) [19], the magnetic field integral equation (MFIE) [19].

Besides, this type of objects can be modeled in SIE by an impedance boundary condition (IBC) on the surface ([13],[4],[5],[1],[18]) . Indeed, the integral electric field equation for a body having an impedance boundary condition can be developed from the equivalence principle by first removing the diffuser from the medium in which it resides and by placing equivalent electric and magnetic surface currents $\mathbf{J}$ and $\mathbf{M}$ along the surface forming the boundary of the scatterer in the original problem ([26],[4],[6],[13]). Among these IBCs are the Leontovitch IBC knowing as the standard impedance boundary condition (SIBC) [27], the higher-order IBC (HOIBC) [28],[29], [13], the generalized IBC (GIBC) [30], [31], etc.

We are interested in solving the scattering problem using SIE formulations with HOIBC [13], which leads to solving a variational problem. The existence and uniqueness of its weak solutions are usually proved by applying arguments. In this paper, we deal with the proof of the existence

and uniqueness theorem of this variational problem using Lax Milgram's theorem that depend on checking the continuity and coercivity of operators that appear in variational problem.
The plan of the paper is the following. In section 2, we present mathematical model and the function space, then we recall the variational problem derived in [13]. We state results on existence and uniqueness of the solution under sufficient conditions to ensure the well-posedness of the variational problem ([13],[4]). In the third section, we propose a new approximation method of operators appeared in the variational problem based on theory of distribution. In a fourth section, numerical experiments are performed to verify the accuracy and efficiency of the proposed method ([6],[5]).

2 Variational approach

To present our variational approach, we will start by offering an overview of the mathematical model of physical problem. For a coated PEC object Ω immersed in an infinite homogeneous medium (ϵ_0, μ_0) and illuminated by an incident uniform plane wave $(\mathbf{E}^{inc}, \mathbf{H}^{inc})$ with angular frequency $\omega = 2\pi f$ (fig. 1), scattering waves occur when incident waves impinge upon the boundary of an object $\Gamma = \partial\Omega$ and disperse in different directions $(\mathbf{E}^{sc}, \mathbf{H}^{sc})$. The extent of scattering depends on both the wavelength λ of the incident waves and the structure of the object (geometry, thickness of coating δ).

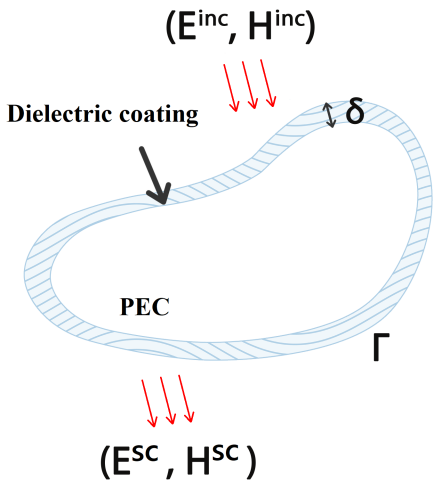

Figure 1: Scattering problem of dielectric coated conducting target

We provide a set of definitions and notations associated with the function spaces that will

be employed in the subsequent analysis.

2.1 Notations and function space

We define the solution space as,

$$V := \{v \in (H^1(\Gamma))^3, v \cdot \mathbf{n} = 0, \mathrm{div}_t\ v \in L^2(\Gamma), \mathrm{rot}_t\ v \in L^2(\Gamma)\}$$

where div_t and rot_t are tangential operators [32], $\mathbf{n}$ denotes the unit normal vector outward to Γ. V generates the norm

$$\|\mathbf{v}\|_V = (\|\mathbf{v}\|^2_{L^2(\Omega)} + \|\mathrm{div}(\mathbf{v})\|^2_{L^2(\Omega)} + \|\mathrm{rot}(\mathbf{v})\|^2_{L^2(\Omega)})^{1/2}$$

usual notation

$$V = H^1_t(\Gamma) \equiv H_{\mathrm{div}}(\Gamma) \cap H_{\mathrm{rot}}(\Gamma)$$

where index 1 denotes one derivative, named after Sobolev and t denotes the tangential vector field. We recall the main properties of Sobolev spaces on Γ [33].

Lemma 2.1. *The injection $H^1_t(\Gamma) \subset L^2_t(\Gamma)$ is compact.*

$$H^1_t(\Gamma) \hookrightarrow L^2_t(\Gamma)$$

Lemma 2.2. *The injection $H^1_t(\Gamma) \subset H^{-1/2}_{\mathrm{div}}(\Gamma)$ is compact.*

$$H^1_t(\Gamma) \hookrightarrow H^{-1/2}_{\mathrm{div}}(\Gamma)$$

with

$$H^{-1/2}_{\mathrm{div}}(\Gamma) = \{\mathbf{g} \in H^{-1/2}(\Gamma)^3,\ \mathbf{g} \cdot \mathbf{n} = 0,\ \mathrm{div}_t(\mathbf{g}) \in H^{-1/2}(\Gamma)\}$$

which we equip with the norm

$$\|\mathbf{g}\|_{H^{-1/2}_{\mathrm{div}}(\Gamma)} = \left(\|\mathbf{g}\|^2_{H^{-1/2}(\Gamma)} + \|\mathrm{div}_t(\mathbf{g})\|^2_{H^{-1/2}(\Gamma)}\right)^{1/2}$$

For any sufficiently regular vector function $\mathbf{A}$, such that $\mathbf{A} \cdot \mathbf{n} = 0$ we define the components of Hodge operator [34] [13]

$$\begin{aligned} L_D : \quad D'(\Gamma)^3 &\to D'(\Gamma)^3 \\ \mathbf{A} &\mapsto \nabla_t(\mathbf{div}_t \mathbf{A}), \end{aligned}$$

$$L_R : \quad D'(\Gamma)^3 \quad \to D'(\Gamma)^3$$
$$\mathbf{A} \qquad \mapsto \mathbf{rot}_t(\mathbf{rot}_t\mathbf{A}).$$

After defining differential operators, integral equations are introduced as the key to establish the variational formulations of diffraction problem.

2.2 Integral equation formulations

The procedure of solving a given problem in electromagnetics typically involves several basic steps. First, it is necessary to express in mathematical form the relationship between the pertinent physical quantities involved. This mathematical description is accomplished through Maxwell's equations, expressed in either integral or differential form. We define Ω^e as the space of radiating electric fields $\mathbf{E}$ solutions of Maxwell's equations that govern this problem.
An electric field is said to be radiating if it satisfies the Silver-Müller radiation condition [35][36]:

$$\lim_{r\to\infty} r(\mathbf{E}\times\mathbf{n}_r + \mathbf{H}) = 0,$$

where $r = |\mathbf{x}|$ and $\mathbf{n}_r = \dfrac{\mathbf{x}}{|\mathbf{x}|}$, $\mathbf{x}\in\mathbb{R}^3$.
The dielectrically coated conducting objects fig. 1 can be modeled by an impedance boundary condition (IBC) at the surface, we are interested in higher-order impedance boundary conditions (HOIBC) (1), (see [13]), various methods are presented for computing the coefficients (a_0, a_j, b_j).

$$(I + b_1L_D - b_2L_R)\mathbf{E}_t = (a_0I + a_1L_D - a_2L_R)(\mathbf{n}\times\mathbf{H}). \tag{1}$$

Thus leading to the following problem:

Problem 2.1. *Find* $(\boldsymbol{E}, \boldsymbol{H})$ *such as*

$$\begin{cases} \nabla\times\boldsymbol{E} + i\omega\mu\boldsymbol{H} = 0 \quad in \quad \Omega^e, \\ \nabla\times\boldsymbol{H} - i\omega\epsilon\boldsymbol{E} = 0 \quad in \quad \Omega^e, \\ (I + b_1L_D - b_2L_R)\boldsymbol{E}_t = (a_0I + a_1L_D - a_2L_R)(\mathbf{n}\times\boldsymbol{H}) \quad in \ \ \Gamma, \\ \lim\limits_{r\to\infty} r(\boldsymbol{E}\times\boldsymbol{n}_r + \boldsymbol{H}) = 0. \end{cases} \tag{2}$$

Based on the equivalence principle, the problem 2.1 can be formulated using integral equations that govern it through the fundamental theorem of Stratton-Chu representation [37], known as the electric and magnetic field integral equations EFIE (3) and MFIE (4) respectively. According to this theorem, waves can be parameterized using electromagnetic operators $(B-S)$ and $(P+Q)$ and their equivalent electric and magnetic current on Γ, $\mathbf{M} = \mathbf{E}\times\mathbf{n}|_\Gamma$ and $\mathbf{J} =$

$\mathbf{n} \times \mathbf{H}|_\Gamma$, as follows.

$$< Z_0(B-S)\mathbf{J}, \mathbf{\Psi}_J > + < (P+Q)\mathbf{M}, \mathbf{\Psi}_J >=< E^{inc}, \mathbf{\Psi}_J >, \tag{3}$$

$$- < (P+Q)\mathbf{J}, \mathbf{\Psi}_M > + < \frac{1}{Z_0}(B-S)\mathbf{M}, \mathbf{\Psi}_M >=< H^{inc}, \mathbf{\Psi}_M > \tag{4}$$

where the integral operators $(B-S)$ and $(P+Q)$ are defined as follows:

$$< (B-S)\phi, \boldsymbol{\psi} >= i \iint_\Gamma k\, G\, \phi \cdot \boldsymbol{\psi} - \frac{1}{k}\, G\, \nabla_y \cdot \phi\, \nabla_x \cdot \boldsymbol{\psi} \quad dydx, \tag{5}$$

$$< (P+Q)\phi, \boldsymbol{\psi} >= \frac{1}{2} \int_\Gamma \boldsymbol{\psi} \cdot (\mathbf{n} \times \phi) \quad dx + \iint_\Gamma (\boldsymbol{\psi} \times \phi) \cdot \nabla_x G \quad dydx, \tag{6}$$

In (5) and (6), G stands for the Green's function in an infinite homogeneous medium with the wavenumber k.

These representations, (3) and (4), will be useful for constructing and developing the variational formulation proposed in [13], in which it suggests replacing the operator P and incorporating the impedance boundary condition (HOIBC) to obtain the variational problem below.

Problem 2.2. *Find $U = (\mathbf{J}, \mathbf{M}) \in V = [H_{\mathrm{div}}(\Gamma) \cap H_{\mathrm{rot}}(\Gamma)]^2$ such that:*

$$A(U, \Psi) =< I\mathbf{E}^{inc}, \mathbf{\Psi}_J > + < I\mathbf{H}^{inc}, \mathbf{\Psi}_M > \tag{7}$$

for all $\mathbf{\Psi} = (\mathbf{\Psi}_J, \mathbf{\Psi}_M) \in V$, with the bilinear form $A(U, \Psi)$ is defined by :

$$A(U, \Psi) =< Z_0(B-S)\boldsymbol{J}, \mathbf{\Psi}_J > + \frac{1}{Z_0} < (B-S)\boldsymbol{M}, \mathbf{\Psi}_M > + < Q\boldsymbol{M}, \mathbf{\Psi}_J > - < Q\boldsymbol{J}, \mathbf{\Psi}_M >$$

$$+ \frac{a_0}{2} < \boldsymbol{J}, \mathbf{\Psi}_J > + \frac{1}{2a_0} < \boldsymbol{M}, \mathbf{\Psi}_M > - \frac{a_1}{2} < \mathrm{div}_\Gamma \boldsymbol{J}, \mathrm{div}_\Gamma \mathbf{\Psi}_J > - \frac{b_2}{2a_0} < \mathrm{div}_\Gamma \boldsymbol{M}, \mathrm{div}_\Gamma \mathbf{\Psi}_M >$$

$$+ \frac{b_1}{2} < \mathrm{div}_\Gamma(\mathbf{n} \times \boldsymbol{M}), \mathrm{div}_\Gamma \mathbf{\Psi}_J > - \frac{b_2}{2} < \mathrm{div}_\Gamma \boldsymbol{M}, \mathrm{div}_\Gamma(\mathbf{n} \times \mathbf{\Psi}_J) > - \frac{b_1}{2a_0} < \mathrm{div}_\Gamma(\mathbf{n} \times \boldsymbol{M}), \mathrm{div}_\Gamma(\mathbf{n} \times \mathbf{\Psi}_M) >$$

$$+ \frac{a_1}{2a_0} < \mathrm{div}_\Gamma \boldsymbol{J}, \mathrm{div}_\Gamma(\mathbf{n} \times \mathbf{\Psi}_M) > - \frac{a_2}{2a_0} < \mathrm{div}_\Gamma(\mathbf{n} \times \boldsymbol{J}), \mathrm{div}_\Gamma \mathbf{\Psi}_M > - \frac{a_2}{2} < \mathrm{div}_\Gamma(\mathbf{n} \times \boldsymbol{J}), \mathrm{div}_\Gamma(\mathbf{n} \times \mathbf{\Psi}_J) >$$

To tackle the problem at hand, [13] recommends the use of Lagrange multipliers in their formulation. However, our research underscores a significant advantage achieved by eliminating these Lagrange multipliers, leading to a reduction in the number of unknowns to be resolved. This conspicuous simplification in the model offers several scientific benefits. Firstly, it optimizes computational efficiency and reduces overall complexity, consequently preserving computational resources and time. By diminishing the count of unknowns, our approach furnishes a potentially more resilient method for tackling complex issues.

In the next section, we are going to give an alternative proof that Problem 2.2 is well-posed by

analysing the bilinear form A defined on $V = [H_{\mathrm{div}}(\Gamma) \cap H_{\mathrm{rot}}(\Gamma)]^2$.

3 Well-posedness of variational problem 2.2

The well-posedness of problem 2.2 is guaranteed by satisfying the sufficient uniqueness conditions (SUC) outlined in both the celebrated Lax-Milgram theorem [38] and the Rellich lemma [13]. We will give these sufficient uniqueness conditions (SUC) under which this problem is well-posed.

Theorem 3.1. *The variational problem* 2.2 *admits a unique solution if the coefficients satisfy the following conditions:*

$$\begin{cases} \Re(a_0) > 0, \\ \Re(a_1) < -\frac{|q_1|}{2}, \\ \Re(b_1 a_0^*) < -\frac{|q_1|}{2} \\ \Re(a_2) < -\frac{|q_2|}{2} \\ \Re(b_2 a_0^*) < -\frac{|q_2|}{2} \end{cases} \tag{8}$$

where : $q_1 = b_1|a_0| + a_1^* a_0/|a_0|$ *et* $q_2 = b_2|a_0| + a_2^* a_0/|a_0|$.

In variational theory, the essential tool in showing that the problem 2.2 is well-posed consists in proving both continuity and coerciveness of integral forms defined on suitable function spaces.

3.1 Continuity of the bilinear form A (7)

In order to facilitate the demonstration and application of properties, we decompose the bilinear form into two parts. The first part is associated with the $(B - S)$ and Q operators, while the second part comprises all other higher-order impedance boundary condition (HOIBC) operators. This decomposition allows us to facilitate the demonstration and analysis process by applying properties.

Lemma 3.2. *The operator* $A(U, \Psi)$ *is continuous in* V *for all* $\Psi \in V$.

Proof. Let us first establish the form of the opereator A

$$A(U, \Psi) = A_1(U, \Psi) + A_2(U, \Psi).$$

We will show that

$$|A(U, \Psi)| \leq C\|U\|_V \|\Psi\|_V.$$

We apply the triangle inequality to the operator A_1.

$$|A_1(U,\Psi)| \leq \|Z_0(B-S)\mathbf{J}\|_{H_{\rm rot}^{-1/2}} \|\mathbf{\Psi}_J\|_{H_{\rm div}^{-1/2}} + |Z_0^{-1}| \|(B-S)\mathbf{M}\|_{H_{\rm rot}^{-1/2}} \|\mathbf{\Psi}_M\|_{H_{\rm div}^{-1/2}}$$

$$+\|Q\mathbf{M}\|_{H_{\rm rot}^{-1/2}} \|\mathbf{\Psi}_J\|_{H_{\rm div}^{-1/2}} + \|Q\mathbf{J}\|_{H_{\rm rot}^{-1/2}} \|\mathbf{\Psi}_M\|_{H_{\rm div}^{-1/2}} \leq C_1' \|U\|_{H_{\rm div}^{-1/2}} \|\Psi\|_{H_{\rm div}^{-1/2}}$$

A_1 is continuous in $H_{\rm div}^{-1/2}(\Gamma)$ then in $V = H_{\rm div}(\Gamma) \cap H_{\rm rot}(\Gamma)$ because $V \subset H_{\rm div}^{-1/2}(\Gamma)$. Consequently:

$$|A_1(U,\Psi)| \leq C_1 \|U\|_V \|\Psi\|_V$$

Proceeding similarly as for $|A_1(U,\Psi)|$

$$|A_2(U,\Psi)| \leq \frac{|a_0|}{2} \|\mathbf{J}\|_{H_t^1(\Gamma)} \|\mathbf{\Psi}_J\|_{H_t^1(\Gamma)} + \frac{1}{2|a_0|} \|\mathbf{M}\|_{H_t^1(\Gamma)} \|\mathbf{\Psi}_M\|_{H_t^1(\Gamma)}$$

$$+\|{\rm div}\mathbf{J}\|_{L_t^2(\Gamma)} \left[\frac{|a_1|}{2} \|{\rm div}_\Gamma \mathbf{\Psi}_J\|_{L_t^2(\Gamma)} + \frac{|a_1|}{2|a_0|} \|{\rm rot}_\Gamma \mathbf{\Psi}_M\|_{L_t^2(\Gamma)} \right]$$

$$+\|{\rm rot}\mathbf{J}\|_{L_t^2(\Gamma)} \left[\frac{|a_2|}{2} \|{\rm rot}_\Gamma \mathbf{\Psi}_J\|_{L_t^2(\Gamma)} + \frac{|a_2|}{2|a_0|} \|{\rm div}_\Gamma \mathbf{\Psi}_M\|_{L_t^2(\Gamma)} \right]$$

$$+\|{\rm div}\mathbf{M}\|_{L_t^2(\Gamma)} \left[\frac{|b_2|}{2} \|{\rm rot}_\Gamma \mathbf{\Psi}_J\|_{L_t^2(\Gamma)} + \frac{|b_2|}{2|a_0|} \|{\rm div}_\Gamma \mathbf{\Psi}_M\|_{L_t^2(\Gamma)} \right]$$

$$+\|{\rm rot}\mathbf{M}\|_{L_t^2(\Gamma)} \left[\frac{|b_1|}{2} \|{\rm div}_\Gamma \mathbf{\Psi}_J\|_{L_t^2(\Gamma)} + \frac{|b_1|}{2|a_0|} \|{\rm rot}_\Gamma \mathbf{\Psi}_M\|_{L_t^2(\Gamma)} \right]$$

$$\leq C_2 \|U\|_V \|\Psi\|_V$$

Hence, combining the sum of these two parts shows that :
$|A(U,\Psi)| = |A_1(U,\Psi) + A_2(U,\Psi)| \leq |A_1(U,\Psi)| + |A_2(U,\Psi)| \leq C\|U\|_V \|\Psi\|_V$ with $C = C_1 + C_2$. □

Now, let us show the coercivity of the operator A .

3.2 Coercivity of the operator A (7)

Lemma 3.3. *The bilinear form $A(U,\Psi)$ verifies the inequality of coecivity for all $U \in V = [H_{\rm div}(\Gamma) \cap H_{\rm rot}(\Gamma)]^4$.*

Proof. We have to show that there exists $\alpha > 0$ such that

$$\Re[A(U,U^*)] \geq \alpha \|U\|_V^2, \ \forall U \in V.$$

Using properties of the operators $B-S$ and Q [39], we know that there exists α_1 such that

$$\Re(A_1) = \Re(< Z_0(B-S)\mathbf{J}, \mathbf{J}^* >) + \Re(< Z_0^{-1}(B-S)\mathbf{M}, \mathbf{M}^* >) + \Re(< Q\mathbf{M}, \mathbf{J}^* >) - \Re(< Q\mathbf{J}, \mathbf{M}^* >)$$

$$\Re(A_1) \geq \alpha_1 \left(\|\mathbf{J}\|^2_{H^{-1/2}_{\mathrm{div}}} + \|\mathbf{M}\|^2_{H^{-1/2}_{\mathrm{div}}} \right) \geq 0$$

On the other hand, one can easily prove that

$$\Re(A_2) = \frac{\Re(a_0)}{2}\|\mathbf{J}\|^2_{L^2_t(\Gamma)} + \frac{\Re(a_0)}{2|a_0|^2}\|\mathbf{M}\|^2_{L^2_t(\Gamma)} - \frac{\Re(a_1)}{2}\|\mathrm{div}_\Gamma \mathbf{J}\|^2_{L^2_t(\Gamma)} - \frac{\Re(a_2)}{2}\|\mathrm{rot}_\Gamma \mathbf{J}\|^2_{L^2_t(\Gamma)}$$

$$- \frac{\Re(b_1 a_0^*)}{2|a_0|^2}\|\mathrm{rot}_\Gamma \mathbf{M}\|^2_{L^2_t(\Gamma)} - \frac{\Re(b_2 a_0^*)}{2|a_0|^2}\|\mathrm{div}_\Gamma \mathbf{M}\|^2_{L^2_t(\Gamma)}$$

$$-\Re\left\{ \left(\frac{b_1}{2} + \frac{a_1^*}{2a_0^*} \right) \int_\Gamma \mathrm{rot}_\Gamma \mathbf{M}\ \mathrm{div}_\Gamma \mathbf{J}^* ds \right\} + \Re\left\{ \left(\frac{b_2}{2} + \frac{a_2^*}{2a_0^*} \right) \int_\Gamma \mathrm{rot}_\Gamma \mathbf{J}^*\ \mathrm{div}_\Gamma \mathbf{M} ds \right\} =$$

$$\frac{\Re(a_0)}{2}\|\mathbf{J}\|^2_{L^2_t(\Gamma)} + \frac{\Re(a_0)}{2|a_0|^2}\|\mathbf{M}\|^2_{L^2_t(\Gamma)} - \frac{\Re(a_1)}{2}\|\mathrm{div}_\Gamma \mathbf{J}\|^2_{L^2_t(\Gamma)} - \frac{\Re(a_2)}{2}\|\mathrm{rot}_\Gamma \mathbf{J}\|^2_{L^2_t(\Gamma)}$$

$$- \frac{\Re(b_1 a_0^*)}{2|a_0|^2}\|\mathrm{rot}_\Gamma \mathbf{M}\|^2_{L^2_t(\Gamma)} - \frac{\Re(b_2 a_0^*)}{2|a_0|^2}\|\mathrm{div}_\Gamma \mathbf{M}\|^2_{L^2_t(\Gamma)}$$

$$-\Re\left\{ \int_\Gamma \frac{1}{|a_0|^{1/2}} \left(\frac{b_1}{2} + \frac{a_1^* a_0}{2|a_0|^2} \right)^{1/2} \mathrm{rot}_\Gamma \mathbf{M}\ \cdot |a_0|^{1/2} \left(\frac{b_1}{2} + \frac{a_1^* a_0}{2|a_0|^2} \right)^{1/2} \mathrm{div}_\Gamma \mathbf{J}^* ds \right\}$$

$$+\Re\left\{ \int_\Gamma |a_0|^{1/2} \left(\frac{b_2}{2} + \frac{a_2^* a_0}{2|a_0|^2} \right)^{1/2} \mathrm{rot}_\Gamma \mathbf{J}^* \cdot \frac{1}{|a_0|^{1/2}} \left(\frac{b_2}{2} + \frac{a_2^* a_0}{2|a_0|^2} \right)^{1/2} \mathrm{div}_\Gamma \mathbf{M} ds \right\}$$

we denote by $q_1 = b_1|a_0| + a_1^* a_0/|a_0|$ et $q_2 = b_2|a_0| + a_2^* a_0/|a_0|$, so

$$\Re(A_2) \geq \frac{\Re(a_0)}{2}\|\mathbf{J}\|^2_{L^2_t(\Gamma)} + \frac{\Re(a_0)}{2|a_0|^2}\|\mathbf{M}\|^2_{L^2_t(\Gamma)} +$$

$$\left(-\frac{\Re(a_1)}{2} - \frac{|q_1|}{4} \right) \|\mathrm{div}_\Gamma \mathbf{J}\|^2_{L^2_t(\Gamma)} + \left(-\frac{\Re(a_2)}{2} - \frac{|q_2|}{4} \right) \|\mathrm{rot}_\Gamma \mathbf{J}\|^2_{L^2_t(\Gamma)} +$$

$$\left(-\frac{\Re(b_2 a_0^*)}{2|a_0|^2} - \frac{|q_2|}{4|a_0|^2} \right) \|\mathrm{div}_\Gamma \mathbf{M}\|^2_{L^2_t(\Gamma)} + \left(-\frac{\Re(b_1 a_0^*)}{2|a_0|^2} - \frac{|q_1|}{4|a_0|^2} \right) \|\mathrm{rot}_\Gamma \mathbf{M}\|^2_{L^2_t(\Gamma)}$$

from the theorem 3.1 in which we imposed conditions on the coefficients (8), the operator A_2 becomes:

$$\Re(A_2) \geq \alpha_2 \left(\|\mathbf{J}\|^2_V + \|\mathbf{M}\|^2_V \right)$$

Finally, we have the integer operator A:

$$\Re(A) = \Re(A_1) + \Re(A_2) \geq \alpha_2 \left(\|\mathbf{J}\|^2_V + \|\mathbf{M}\|^2_V \right)$$

□

Eventually, since the bilinear form A is continuous and coercive in V under sufficient con-

ditions, we then arrive at the well-posedness result for our variational formulation according to Lax-Milgram theorem.

In an effort to numerically solve the well-posed variational problem, we now turn our attention towards discretization techniques to approximate the continuous problem on a discrete problem.

4 Discretization and operators' approximation

The obtained variational Problem 7 is solved with the method of moments (MoM) [26] using Galerkin testing procedure, which requires discretizing the contour defining the surface Γ into triangles T.

$$\Gamma_h = \bigcup_{n=1}^{N_T} T_n.$$

To discretize the variational problem, we employ a non-conformal approach, the Galerkin method is employed utilizing RAO-Wilton-Glisson RWG basis functions defined on the space $W = H_{\text{div}}^{-1/2}$, i,e. , the equivalent currents on the surface J and M are approximated on a set of N_e basis functions using RWG functions $f_i(x)$ with the unknown are the flows such as:

$$\mathbf{J}(x) = \sum_{i=1}^{Ne} J_i \mathbf{f}_i(x), \quad \mathbf{M}(x) = \sum_{i=1}^{Ne} M_i \mathbf{f}_i(x). \tag{9}$$

On each triangle, the current is written as a linear combination of 3 functions of base associated with 3 edges of a triangle. If n is a common edge of two triangles then:

$$\mathbf{f}_n(x) = \begin{cases} \frac{l_n}{2|T_n^+|}(x - a_{i-1}^+) & if\ x \in T_n^+ \\ \frac{l_n}{2|T_n^-|}(a_{j-1}^- - x) & if\ x \in T_n^- \\ 0 & if\ x \notin T_n^+ \cup T_n^- \end{cases} \tag{10}$$

we define also its divergence:

$$\nabla_\Gamma \cdot \mathbf{f}_n(x) = \begin{cases} +\frac{l_n}{|T_n^+|} & if\ x \in T_n^+ \\ -\frac{l_n}{|T_n^-|} & if\ x \in T_n^- \\ 0 & if\ x \notin T_n^+ \cup T_n^-. \end{cases} \tag{11}$$

By arbitrary definition, the current flows from the first triangle of the zone T_n^+ to the second triangle of the zone T_n^-. a_{i-1}^+ and a_{j-1}^- are the opposite vertices of the edge n in T_n^+ and T_n^- respectively. $|T_n^\pm|$ designates the area of the triangle $T_n^\pm$ and the length of the common edge is l_n. Through the use of the decomposition of surface electric and magnetic densities (9), we

inject them into the variational problem (2.2).

This procedure converts the coupled set of integral equations into a matrix which may be cast into the form.

$$A^h(U_h, \Psi_h) = \sum_{i=1}^{Ne} < \mathbf{E}^{inc}, \mathbf{f}_i > + \sum_{i=1}^{Ne} < \mathbf{H}^{inc}, \mathbf{f}_i > \tag{12}$$

where

$$A^h(U_h, \Psi_h) = \sum_{i,j=1}^{N_e} < Z_r Z_0 \ (B - S)\mathbf{f}_j, \mathbf{f}_i > J_j + Z_r^{-1} Z_0^{-1} \sum_{i,j=1}^{N_e} < (B - S)\mathbf{f}_j, \mathbf{f}_i > M_j$$

$$+ \sum_{i,j=1}^{N_e} < Q\mathbf{f}_j, \mathbf{f}_i > M_j - \sum_{i,j=1}^{N_e} < Q\mathbf{f}_j, \mathbf{f}_i > J_j + \frac{a_0}{2} \sum_{i,j=1}^{N_e} < \mathbf{f}_j, \mathbf{f}_i > J_j + \frac{1}{2a_0} \sum_{i,j=1}^{N_e} < \mathbf{n}\times\mathbf{f}_j, \mathbf{n}\times\mathbf{f}_i > M_j$$

$$+ \frac{a_1}{2} \sum_{i,j=1}^{N_e} < \nabla_\Gamma \nabla_\Gamma \cdot \mathbf{f}_j, \mathbf{f}_i > J_j - \frac{a_2}{2} \sum_{i,j=1}^{N_e} < \nabla_\Gamma \nabla_\Gamma \cdot (\mathbf{n} \times \mathbf{f}_j), \mathbf{n} \times \mathbf{f}_i > J_j$$

$$- \frac{b_1}{2} \sum_{i,j=1}^{N_e} < \nabla_\Gamma \nabla_\Gamma \cdot \mathbf{f}_j, \mathbf{n} \times \mathbf{f}_i > M_j + \frac{b_2}{2} \sum_{i,j=1}^{N_e} < \nabla_\Gamma \nabla_\Gamma \cdot (\mathbf{n} \times \mathbf{f}_j), \mathbf{f}_i > M_j$$

$$+ \frac{b_1}{2a_0} \sum_{i,j=1}^{N_e} < \nabla_\Gamma \nabla_\Gamma \cdot (\mathbf{n} \times \mathbf{f}_j), \mathbf{n} \times \mathbf{f}_i > M_j - \frac{b_2}{2a_0} \sum_{i,j=1}^{N_e} < \nabla_\Gamma \nabla_\Gamma \cdot \mathbf{f}_j, \mathbf{f}_i > M_j$$

$$- \frac{a_1}{2a_0} \sum_{i,j=1}^{N_e} < \nabla_\Gamma \nabla_\Gamma \cdot (\mathbf{n} \times \mathbf{f}_j), \mathbf{f}_i > J_j + \frac{a_2}{2a_0} \sum_{i,j=1}^{N_e} < \nabla_\Gamma \nabla_\Gamma \cdot \mathbf{f}_j, \mathbf{n} \times \mathbf{f}_i > J_j;$$

We seek an approximate solution to the discrete problem (12). To solve it, we first give notations for the integral operators arising from the Higher-Order Integral Boundary Conditions (HOIBC) involved in the discrete problem, defined as follows:

$$L_{ij} = \int_{\Gamma_h} \mathbf{f}_i \cdot \mathbf{f}_j ds, \tag{13}$$

$$D_{ij} = \int_{\Gamma_h} \nabla_\Gamma \nabla_\Gamma \cdot \mathbf{f}_j \cdot \mathbf{f}_i ds \tag{14}$$

$$E_{ij} = \int_{\Gamma_h} \nabla_\Gamma \nabla_\Gamma \cdot \mathbf{f}_j \cdot \mathbf{n} \times \mathbf{f}_i ds, \tag{15}$$

$$G_{ij} = \int_{\Gamma_h} \nabla_\Gamma \nabla_\Gamma \cdot (\mathbf{n} \times \mathbf{f}_j) \cdot \mathbf{n} \times \mathbf{f}_i ds. \tag{16}$$

The RWG function is not suitable for all terms present in the formulation, because the divergence of the RWG function is piecewise constant (11). Hence the tangential gradient of divergence is not defined, it gives us the Dirac function on the edges of the two elements in the operators which have $\nabla_\Gamma \nabla_\Gamma \cdot$ in the integral like the operators D (14), E (15) and G (16).

The presence of discontinuous functions in integral operators arising from high-order impedance boundary conditions can introduce challenges in the analysis of such operators. Because of these

observed drawbacks, it may be interesting to make an approximation of these operators using more elaborate approaches.

Jump formulas are indeed a valuable tool for addressing the challenges posed by these discontinuous functions, and their utilization becomes imperative as they provide an effective solution to prevent inaccuracies in computations.

4.1 The jump formula

Definition 4.1. *Formula for the jump across a bounded surface*

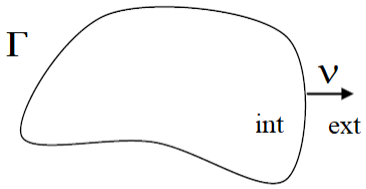

Let Ω be an open set of $\mathbb{R}^3$, with a Lipschitz boundary Γ, F a regular function in $\mathbb{R}^3$, such that C^1-regular on either side of Γ. Then the jump of the discontinuous function F through Γ is denoted by:

$$[F]_\Gamma = F^{int} - F^{ext}$$

with F^{int}, F^{ext} are the values of F inside and outside the domain bounded by Γ respectively. The normal $\boldsymbol{\nu}$ to Γ is oriented inside out.

This definition leads to the formulas of the gradient and the divergence in the sense of distribution for functions which are discontinuous at this interface:

Proposition 4.2. *With the regularity hypotheses of the function F, we have:*
The gradient and the divergence in the sense of the distributions defined for functions which are discontinuous at an interface Γ are given by:

$$\nabla F = (\nabla F) - S_\Gamma([F]\boldsymbol{\nu}) \tag{17}$$

$$\nabla \cdot F = (\nabla \cdot F) - S_\Gamma([F \cdot \boldsymbol{\nu}]) \tag{18}$$

where (∇F) and $(\nabla \cdot F)$ are respectively the usual gradient and divergence of the function where they exist and S_Γ is the operator defined by:

$$< S_\Gamma(F), \varphi >= \int_\Gamma F(x)\varphi(x)\, dx.$$

One observes the presence of discontinuity through the edges which deteriorates the conditioning of the operators, an approximation method is thus necessary.
According to (17) the gradient of piecewise constant functions F is written in this form:

$$< \nabla_\Gamma F, \varphi >= -[F]_{/\Gamma} \int_\Gamma \boldsymbol{\nu}(x) \cdot \varphi(x)\, dx\ , \quad \forall \varphi \in D(\mathbb{R}^3)^3 \tag{19}$$

one has upon the application of $F = \nabla_\Gamma \cdot \mathbf{f}$ in (19), so that $< \nabla_\Gamma \nabla_\Gamma \cdot f, \varphi >$ can be written as

$$< \nabla_\Gamma \nabla_\Gamma \cdot \mathbf{f}, \varphi >= -[\nabla_\Gamma \cdot \mathbf{f}]_{/\Gamma} \int_\Gamma \boldsymbol{\nu}(x) \cdot \varphi(x)\, dx\ , \quad \forall \varphi \in D(\mathbb{R}^3)^3 \tag{20}$$

By taking the triangles as the domain of calculation, we have Dirac masses which will appear on the edges of the edges of the triangles because the divergence of the functions of RWG are constant per triangle (11).
The subtitution of this equation (20) into integral HOIBC operators will yield a well-conditionned integrals.

4.2 Integral operators' approximation

To have an explicit expression of the operators, we first define the jump of a piecewise constant function f with respect to an edge i [4].

Definition 4.3. *The jump of a piecewise constant function f with respect to an edge i:*

$$\begin{aligned} [\boldsymbol{f}]_{/i} &= (\varepsilon_i f)^{T_i^+} + (\varepsilon_i f)^{T_i^-} \\ &= \varepsilon_i^{T_i^+} f^{T_i^+} + \varepsilon_i^{T_i^-} f^{T_i^-} \\ &= f^{T_i^+} - f^{T_i^-} \end{aligned}$$

with the trace of f on T_i^+ and T_i^- denoted by $f^{T_i^+}$ and $f^{T_i^-}$ respectively.
The function ε_i is defined by:

$$\varepsilon_i(x) = \begin{cases} 1 \quad on \quad T_i^+, \\ -1 \ on \quad T_i^-, \\ 0 \quad otherwise. \end{cases}$$

4.2.1 Approximation of operator D

We will explain the method of calculating the elements of matrices D_{ij}. By applying the differential operators property (20) to the D operator [4]:

$$\begin{aligned} D_{ij} &= \int_{\Gamma_h} \nabla_\Gamma \nabla_\Gamma \cdot \mathbf{f}_j \cdot \mathbf{f}_i \, dS \\ &= -l_i [\nabla \cdot \mathbf{f}_j]_{/l} \int_l \boldsymbol{\nu}_l \cdot \mathbf{f}_i \, ds \end{aligned}$$

with $\boldsymbol{\nu}_l^+$ (respectively $\boldsymbol{\nu}_l^-$) is the outgoing normal to edge l which goes from T_l^+ to T_l^- (respectively from T_l^- to T_l^+) in the plane of the triangle.
We deduce the expression of the operator D_{ij}:

$$D_{ij} = -\, l_i [\nabla \cdot \mathbf{f}_j]_{/i}. \tag{21}$$

Using definition 4.1, the divergence jump of RWG functions (10):

$$\begin{aligned} \left[\nabla \cdot \mathbf{f}_j\right]_{/i} &= \left[(\varepsilon_i \nabla \cdot \mathbf{f}_j)^{T_i^+} + (\varepsilon_i \nabla . \mathbf{f}_j)^{T_i^-}\right] && (22) \\ &= {\varepsilon_i}^{T_i^+} \nabla \cdot {\mathbf{f}_j}^{T_i^+} + {\varepsilon_i}^{T_i^-} \nabla \cdot {\mathbf{f}_j}^{T_i^-} && (23) \\ &= \varepsilon_i^{T_i^+} \varepsilon_j^{T_i^+} \frac{l_j}{|T_j|^{T_i^+}} + \varepsilon_i^{T_i^-} \varepsilon_j^{T_i^-} \frac{l_j}{|T_j|^{T_i^-}} && (24) \end{aligned}$$

so the D_{ij} (21) can therefore be written as

$$D_{ij} = -l_i \left(\varepsilon_i^{T_i^+} \varepsilon_j^{T_i^+} \frac{l_j}{|T_j|^{T_i^+}} + \varepsilon_i^{T_i^-} \varepsilon_j^{T_i^-} \frac{l_j}{|T_j|^{T_i^-}} \right).$$

4.2.2 Approximation of operator E

Similarly as for the operator D, using the definition of the gradient of piecewise constant function, the operator E can be written as :

$$\begin{aligned} E_{ij} &= \int_{\Gamma_h} \nabla_\Gamma \nabla_\Gamma \cdot \mathbf{f}_j \cdot \mathbf{n} \times \mathbf{f}_i \, ds \\ &= -\sum_{l=1}^{Ne} \left[\nabla \cdot \mathbf{f}_j\right]_{/l} \int_l \boldsymbol{\nu}_l \cdot \mathbf{n} \times \mathbf{f}_i \, ds \end{aligned}$$

We make an approximation of $\int_l \boldsymbol{\nu}_l \cdot \mathbf{n} \times \mathbf{f}_i \, ds$ to translate the discontinuity of the normals which is:

$$\int_l \boldsymbol{\nu}_l \cdot \mathbf{n} \times \mathbf{f}_i \, ds = \frac{1}{2} \left(\int_l \boldsymbol{\nu}_l \cdot \mathbf{n} \times \mathbf{f}_i \, ds \right)_{T_i^+} + \frac{1}{2} \left(\int_l \boldsymbol{\nu}_l \cdot \mathbf{n} \times \mathbf{f}_i \, ds \right)_{T_i^-} \tag{25}$$

To determine this integral, it is necessary to distinguish several geometric configurations.

$$\int_l \boldsymbol{\nu}_l \cdot \mathbf{n} \times \mathbf{f}_i \, ds = \begin{cases} \frac{1}{2}(\int_l \boldsymbol{\nu}_l^+ \cdot \mathbf{n}_{T_i^+} \times \mathbf{f}_i^+ \, ds + \int_l \boldsymbol{\nu}_l^- \cdot \mathbf{n}_{T_i^-} \times \mathbf{f}_i^- \, , ds), & \text{if } i = l \\ \frac{1}{2} \int_l \boldsymbol{\nu}_l^+ \cdot \mathbf{n}_{T_l^+} \times \mathbf{f}_i^{\pm} \, ds, & \text{if } i \in T_l^+ \\ \frac{1}{2} \int_l \boldsymbol{\nu}_l^- \cdot \mathbf{n}_{T_l^-} \times \mathbf{f}_i^{\pm} \, ds, & \text{if } i \in T_l^- \end{cases}$$

The expression of the operator E is then written:

$$\begin{aligned} E_{ij} &= -\frac{1}{2}([\nabla.\mathbf{f}_j]_{/i} \left(\int_{l=i} \boldsymbol{\nu}_i^+ \cdot \mathbf{n}_{\mathbf{T_i^+}} \times \mathbf{f}_i^+ \, ds + \int_{l=i} \boldsymbol{\nu}_i^- \cdot \mathbf{n}_{T_i^-} \times \mathbf{f}_i^- \, ds \right) \\ &+ \sum_{l \in T_i^+ = T_l^+} [\nabla.\mathbf{f}_j]_{/l} \int_l \boldsymbol{\nu}_l^+ \cdot \mathbf{n}_{T_l^+} \times \mathbf{f}_i^+ \, ds + \sum_{l \in T_i^+ = T_l^-} [\nabla.\mathbf{f}_j]_{/l} \int_l \boldsymbol{\nu}_l^- \cdot \mathbf{n}_{\mathbf{T_l^-}} \times \mathbf{f}_i^+ \, ds \\ &+ \sum_{l \in T_i^- = T_l^+} [\nabla.\mathbf{f}_j]_{/l} \int_l \boldsymbol{\nu}_l^+ \cdot \mathbf{n}_{T_l^+} \times \mathbf{f}_i^- \, ds + \sum_{l \in T_i^- = T_l^-} [\nabla.\mathbf{f}_j]_{/l} \int_l \boldsymbol{\nu}_l^- \cdot \mathbf{n}_{T_l^-} \times \mathbf{f}_i^- \, , ds). \end{aligned}$$

The integral operator which is defined by:

$$\int_{\Gamma_h} L_D(\mathbf{n} \times \mathbf{f}_j) \cdot \mathbf{f}_i \, ds$$

is the adjoint operator of operator E_{ij}.

4.2.3 Approximation of the G operator

Employing the definition of the operator G and the jump formula, we deduce the result for the operator E using similar procedure, we find [5]:

$$\begin{aligned} G_{ij} &= \int_{\Gamma_h} \nabla_\Gamma \nabla_\Gamma \cdot (\mathbf{n} \times \mathbf{f}_j) \cdot (\mathbf{n} \times \mathbf{f}_i) \, ds \\ &= -\frac{1}{2}([\nabla.(\mathbf{n} \times \mathbf{f}_j)]_{/i} \left(\int_{l=i} \boldsymbol{\nu}_i^+ \cdot \mathbf{n}_{\mathbf{T_i^+}} \times \mathbf{f}_i^+ \, ds + \int_{l=i} \boldsymbol{\nu}_i^- \cdot \mathbf{n}_{T_i^-} \times \mathbf{f}_i^- \, ds \right) \\ &+ \sum_{l \in T_i^+ = T_l^+} [\nabla.(\mathbf{n} \times \mathbf{f}_j)]_{/l} \int_l \boldsymbol{\nu}_l^+ \cdot \mathbf{n}_{T_l^+} \times \mathbf{f}_i^+ \, ds + \sum_{l \in T_i^+ = T_l^-} [\nabla.(\mathbf{n} \times \mathbf{f}_j)]_{/l} \int_l \boldsymbol{\nu}_l^- \cdot \mathbf{n}_{\mathbf{T_l^-}} \times \mathbf{f}_i^+ \, ds \\ &+ \sum_{l \in T_i^- = T_l^+} [\nabla.(\mathbf{n} \times \mathbf{f}_j)]_{/l} \int_l \boldsymbol{\nu}_l^+ \cdot \mathbf{n}_{T_l^+} \times \mathbf{f}_i^- \, ds + \sum_{l \in T_i^- = T_l^-} [\nabla.(\mathbf{n} \times \mathbf{f}_j)]_{/l} \int_l \boldsymbol{\nu}_l^- \cdot \mathbf{n}_{T_l^-} \times \mathbf{f}_i^- \, ds). \end{aligned}$$

The jump calculation $[\nabla \cdot (\mathbf{n} \times \mathbf{f}_j)]_{/l}$ is based on the calculation of the adjoint operator of E.

5 Numerical experiments

In this section, several examples will be presented to show the accuracy of the proposed method and correctness of the developed formulation after implementing it into MoM code ([5],[6]). A standard spherical coordinate system is used for the body of revolution model with the z axis being the axis of revolution. Several geometries and different types of dielectric material (electric permittivity ϵ_r and magnetic permeability μ_r) are also presented. The first example is considered for validating the accuracy of the code developed while the remaining examples are regarded to produce some new results which cannot be found elsewhere in literature.

First, we consider a coated conductive sphere having a radius of $r_2 = 1.8\lambda$, thickness of coating layer is $0.05m$ (fig. 2) with a relative permittivity of $\epsilon_r = 5$ and a relative permeability of $\mu_r = 1$. The exact series-solution of this geometry is available and is used here to validate the results of the proposed formulation. The bistatic RCS for the $\theta\theta$-polarization at $0.45GHz$ are computed and the results obtained (fig. 3) are compared with Mie series solutions. Figure 3 illustrates three results, Mie's analytical result and different mesh densities using the new approximation method. Good agreements have been observed in the comparisons.

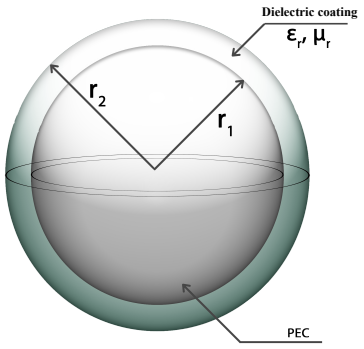

Figure 2: geometry of a coated conductive sphere

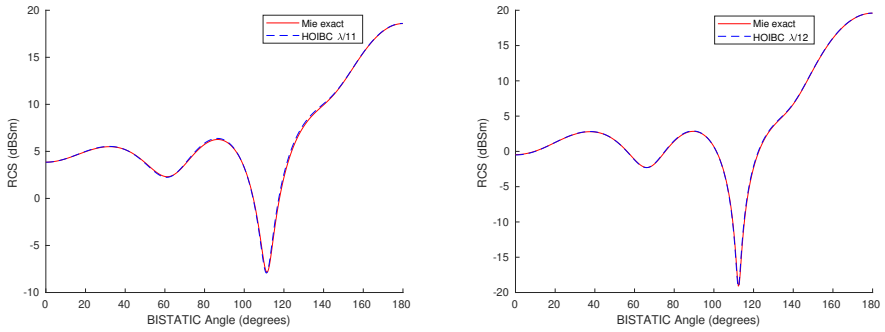

(a) $\epsilon_r = 1 - i$ and $\mu_r = 1$ (b) $\epsilon_r = 2 - 3i$ and $\mu_r = 1 - i$

Figure 4: $\theta\theta$ component of the bistatic RCS for a coated conductive sphere with frequency $f = 0.190986GHz$, layer thickness $\delta \simeq 0.05\lambda$. Exact Mie solution and HOIBC solution

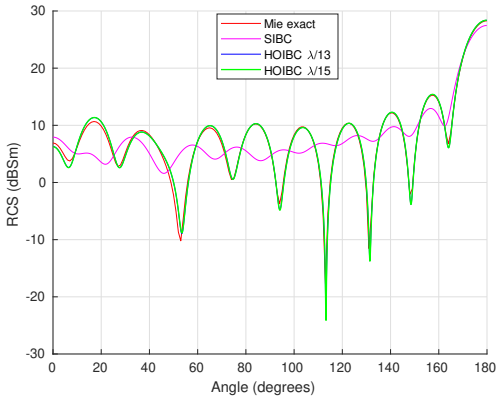

Figure 3: $\theta\theta$ component of the bistatic RCS for a coated conductive sphere with frequency $f = 0.45GHz$, layer thickness $\delta = 0.09\lambda$. Exact Mie solution and HOIBC solutions.

Now, we will choose a complex configurations of permittivity and permeability. In fig. 4a and fig. 4b, when we substitute the complex values for permeability and permittivity, we observe a very good agreement between the analytical solution of Mie and the numerical results obtained using the HOIBC method. In our study, we compared our method to the Lagrange multiplier method proposed in [13]. Since the analytical solution is available for comparison, we computed the error for different meshes using the infinity norm for both methods. Additionally, we measured the CPU time (in seconds) for system resolution and the total memory occupation of the matrix (in Go). We begin by considering the case where $\epsilon_r = 5$ and $\mu_r = 1$.

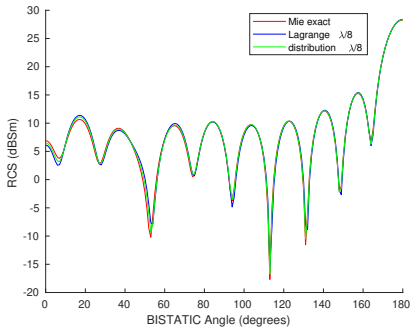

(a) Comparison between Lagrange solution and distribution solution of the corresponding mesh $\lambda/8$. The Mie series solution is used as reference data.

number of unknowns	mesh density	Distribution			Lagrange		
		$\|.\|_\infty$	CPU(s)	Mem(Go)	$\|.\|_\infty$	CPU(s)	Mem(Go)
55788	$\lambda/8$	0.018	343.66	27.2	0.032	385.7	27.2
101760	$\lambda/10$	0.018	1287.16	84.81	0.032	1365.9	84.81
125376	$\lambda/11$	0.0152	2326.97	118.37	0.032	2602.63	118.37
186684	$\lambda/14$	0.0104	4529.9	285.16	0.031	4736.36	285.16

(b) Comparison in terms of relative error and memory usage with respect to mesh density

Figure 5: Values of error computed using two approximations of integral operators with the different mesh with $\epsilon_r = 5$ and $\mu_r = 1$.

In fig. 5a, it is evident that the results of both methods compare well with the exact solution. But, from the above discussion in fig. 5b, we can see that the other method suffers a drastic increase in the computation cost as the number of unknowns increases. The matrix size, and hence, both the filling and solving times grow substantially. On the other hand, our method has a better performance regarding the CPU times where the computation cost is substantially lower. In the light of these factors, our method is more appealing than the other formulation for simulating large-scale problems where the reduction of CPU times becomes an essential and crucial issue. Now we compute the error with complex permitivity and permeability $\epsilon_r = 2 - 3i$ and $\mu_r = 1 - i$.

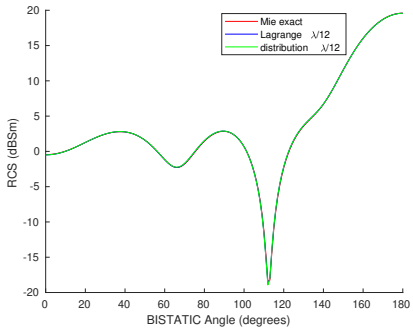

(a) Comparison between Lagrange solution and distribution solution for the mesh $\lambda/12$.

number of unknowns	mesh density	Distribution			Lagrange		
		$\|.\|_\infty$	CPU(s)	Mem(Go)	$\|.\|_\infty$	CPU(s)	Mem(Go)
4956	$\lambda/8$	0.013	1.9	0.32	0.0122	1.95	0.32
10824	$\lambda/12$	0.0051	11.69	1.32	0.0039	12.75	1.32
44664	$\lambda/25$	0.005	54.28	19.26	0.0026	76.05	19.26

(b) Comparison in terms of error and memory usage with respect to mesh density

Figure 6: Values of relative error computed using two approximations of integral operators with the different mesh with $\epsilon_r = 2 - 3i$ and $\mu_r = 1 - i$.

According to the tests presented above, it can be concluded that Lagrange approximation has a good accuracy independently with respect to the number of unknowns, while our approximation has the best performance in terms of computational cost.

We will now transition to a different geometry where no analytical scattering solution is available as a reference. To obtain the reference results, we compare our method to the reference PMCHWT formulation ([8],[9],[10]). We move on to the case of an ellipsoid is with dielectric parameters as depicted in fig. 7a, we choose a coating thickness $\delta = 0.1\lambda$.

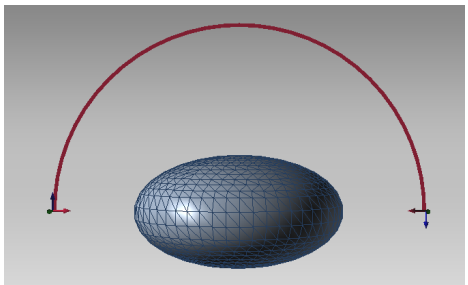

(a) Surfacic mesh of the ellipsoid. $\epsilon_r = 5$ and $\mu_r = 1$.

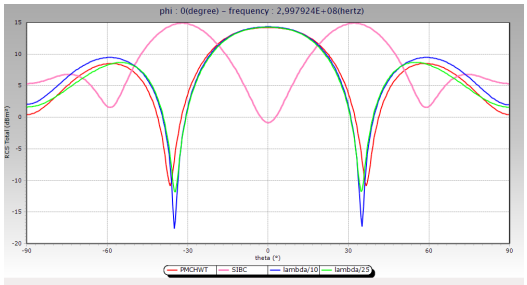

(b) $\theta\theta$ component of the monostatic RCS with frequncy $f = 0.3GHz$. Reference PMCHWT and HOIBC solutions.

Figure 7a presents surface mesh of ellipsoid geometry and fig. 7b plots $\theta\theta$ component of the monostatic RCS with the solution using SIBC and two mesh densities $\lambda/10$ and $\lambda/25$ and we compare it to PMCHWT reference. We notice that we obtain a good accuracy compared with the reference PMCHWT when we use a finer mesh.

In the sequel, sharp-edged targets will be simulated by the suggested method to verify the stability of the proposed formulation. We consider the case of coated PEC almond. Its total length is $4.169\lambda_0$, where λ_0 is the vacuum wavelength, and the dielectric parameters are $\epsilon_r = 4$ and $\mu_r = 1$. A 0.5-GHz monostatic RCS, $\theta\theta$-polarized incident wave is incident from the tip of the almond. Figure 8a shows the mesh configuration of this problem fig. 8b.

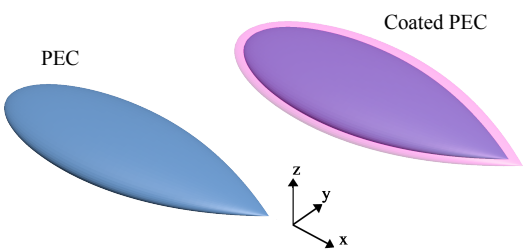

(a) Problem description

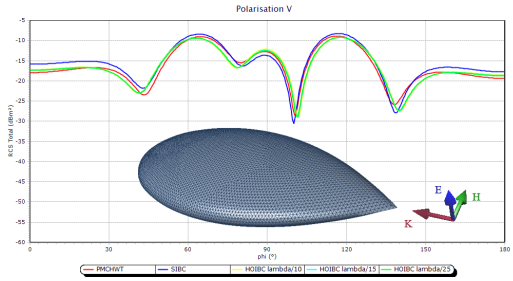

(b) Surface mesh for nasa almond geometry. Plot of SIBC , HOIBC with different mesh density and PMCHWT reference

Figure 8: Scattering analysis for the NASA almond with $\epsilon_r = 4$ and $\mu_r = 1$. A 0.5-GHz monostatic RCS, $\theta\theta$-polarized incident wave is incident from the tip of the almond

Figure 8b plots different HOIBC mesh densities solutions and SIBC solution. It is clear that HOIBC converge to PMCHWT reference and more accurate compared to SIBC.

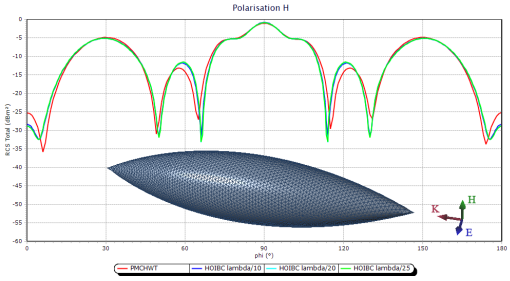

(a) Surface mesh for simple-ogival geometry. Plot HOIBC with different mesh density and PMCHWT reference

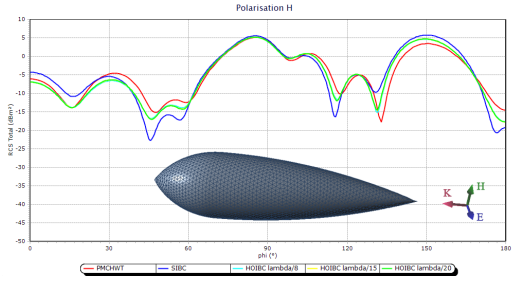

(b) Surface mesh for double-ogival geometry. Plot of SIBC , HOIBC with different mesh density and PMCHWT reference

Figure 9: Scattering analysis for different types of ogives (double fig. 9a and simple fig. 9b). A monostatic RCS, $\phi\phi$-polarized incident wave is incident from the tip of the ogives

Based on the tests on the sphere (see fig. 2), ellipsoid (see fig. 7a), and double-ogive (see fig. 9b), it can be concluded that the Higher Order Impedance Boundary Condition (HOIBC)

approximation exhibits good accuracy. However, the Standard Impedance Boundary Condition (SIBC) approximation demonstrates poor accuracy in both simple and complex cases.

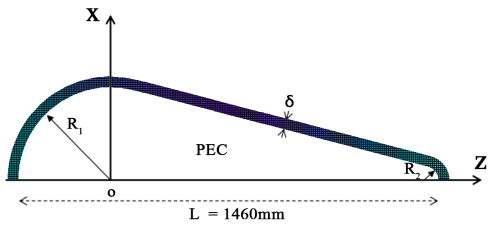

(a) Geometry of coated conductive sphere-cone-sphere.$R_1 = 315mm, R2 = 50mm$.
$\delta = 0.02m$, $\epsilon_r = 5$ and $\mu_r = 1$.

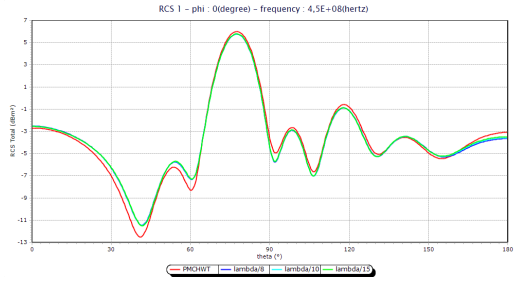

(b) $\phi\phi$ component of the monostatic RCS with frequency $f = 0.45GHz$. Reference PMCHWT and HOIBC solutions.

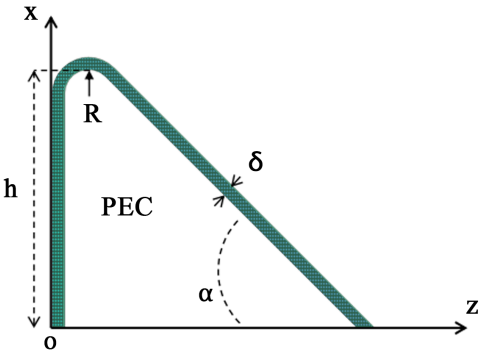

(c) Geometry of cone. $h = 716mm$, $R = 66mm$, $\alpha = 45°$ and $\delta = 0.034m$, $\epsilon_r = 2 - i$ and $\mu_r = 1$.

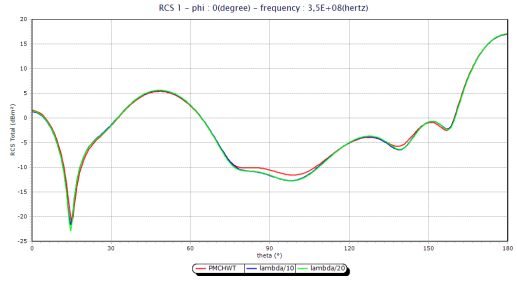

(d) $\phi\phi$ component of the monostatic RCS with frequency $f = 0.35GHz$. Reference PMCHWT and HOIBC solutions.

Figure 10: Performance comparison of different mesh of HOIBC formulation with respect to PMCHWT reference of conic geometries

Figure 10a and fig. 10c presents geometrical parameters of coated conductive sphere-cone-sphere and coated conductive cone respectively. Figure 10b and fig. 10d plots $\phi\phi$ component of the monostatic RCS with different mesh densities and frequencies compared with PMCHWT reference. We observe that, in both geometries,increasing the number of unknowns yields good accuracy regardless of the frequency. As shown in fig. 10d, the two curves of HOIBC solutions agree excellently with each other comparing to the reference.

We choose now another conic geometry (fig. 11) that is coated with a complex homogeneous material layer $\epsilon_r = 1 - i$ and $\mu_r = 1$.

Figure 11a shows the mesh configuration of cone and fig. 11b display the results obtained. We can observe that as the mesh density increases, the HOIBC solutions exhibit a strong agreement with the reference PMCHWT. This can be attributed to the excellent performance of the HOIBC operators employed in the formulation.

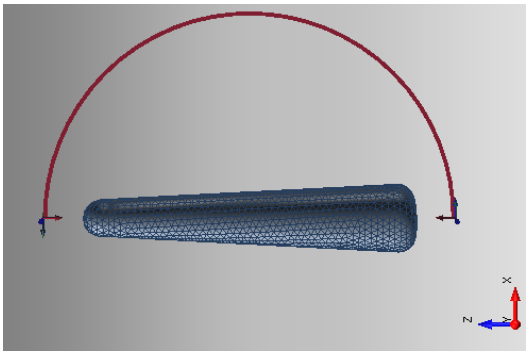

(a) Monostatic RCS of a $1.312m \times 1.312m \times 0.798m$ of a coated PEC cone body ($\delta = 0.05m$, $\epsilon_r = 1 - i$ and $\mu_r = 1$) at $0.19GHz$.

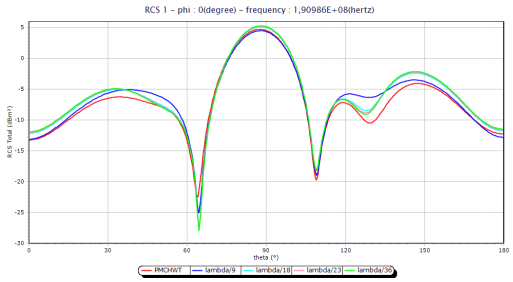

(b) $\theta\theta$ RCS component. Reference PMCHWT and HOIBC solutions.

Figure 11: Performance comparison of different mesh of HOIBC formulation with respect to PMCHWT reference

We gave some preliminary results indicating good accuracy behavior of our method compared to the popular PMCHWT equation. Numerical examples demonstrate that the developed new formulation lead to clear improvements in the convergence rates.

6 Conclusion

In this paper, we have proposed and analyzed a new method for approximating operators resulting from the formulation of the scattering problem by coated 3-D arbitrary shaped objects. We have demonstrated that this formulation is well-posed and implemented it in a MoM code coupled with our method. Numerical comparisons with the commonly used PMCHWT formulation have highlighted the efficiency of our new approach.

In conclusion, our method presents a promising alternative to classical formulations (SIBC) in the context of coated obstacles, offering improved efficiency and accuracy.

References

[1] A. Aubakirov C. Daveau and P. Soudais. High order impedance boundary condition for mom scattering. *International Journal of Numerical Analysis and Modeling*, 2022.

[2] C. Daveau S. Oueslati, I. Balloumi and A. Khelifi. Analytical method for the evaluation of singular integrals arising from boundary element method in electromagnetism. *International Journal of Numerical Modelling: Electronic Networks, Devices and Fields*, 2021.

[3] C. Daveau and J. Laminie. Mixed and hybrid formulations for the three-dimensional magnetic problem. *Numerical Methods for Partial Differential Equations*, Vol. 18:pages 85–104, Jan 2002.

[4] S. Oueslati. *A new variational formulation for electromagnetic scattering problem using integral method with high order impedance boundary condition - Small perturbations of an interface for Stokes system.* PhD thesis, CY Paris Université, 2019.

[5] M. Kacem. *Méthode intégrale avec une condition d'impédance d'ordre élevé pour résoudre le problème de Maxwell en régime harmonique.* PhD thesis, CY Cergy Paris Université, 2022.

[6] C. Daveau, M. Kacem, S. Oueslati, and S. Bornhofen. Higher order impedance boundary condition with integral method for the scattering problem in electromagnetism. *International Conference on PhotonIcs and Electromagnetics Research Symposium (PIERS)*, 2021.

[7] S. Oueslati C. Daveau, A. Aubakirov and C. Carre. Boundary element method with high order impedance boundary condition for maxwell's equations. *Applied Mathematical Modelling*, Vol.118:53–70, 2023.

[8] L. N. Medgyesi-Mitschang P. L. Huddleston and J. M. Putnam. Combined field integral equation formulation for scattering by dielectrically coated conducting bodies. *IEEE Transactions on Antennas and Propagation*, 1986.

[9] M. Taskinen Ylä-Oijala and S. Järvenpää. Surface integral equation formulations for solving electromagnetic scattering problems with iterative methods. *Radio science*, 2005.

[10] J. Jin S. Yan and Z. Nie. A comparative study of calderón preconditioners for PMCHWT equations. *IEEE Transactions on Antennas and Propagation*, 2010.

[11] F. Wübbeling F. Natterer. A finite difference method for the inverse scattering problem at fixed frequency. *Chapter in Lecture Notes in Physics-Reseach Gate*, Vol. 6(No 1):pages 157–166, January 2006.

[12] T. Nguyen H. Haddar. *A volume integral method for solving scattering problems from locally perturbed infinite periodic layers.* HAL, second edition edition, 2016.

[13] A. Aubakirov. *Electromagnetic Scattering Problem with Higher Order Impedance Boundary Conditions and Integral Methods.* Thèse de doctorat, Université Cergy Pontoise, 2014.

[14] V. V. Liepa J. M. Jin and C. T. Tai. A volume-surface integral equation for electromagnetic scattering by inhomogeneous cylinders. *Journal of Electromagnetic Waves and Applications*, 1988.

[15] E. A. Soliman A. A. Sakr and A. K. Abdelmageed. An integral equation formulation for TM scattering by a conducting cylinder coated with an inhomogeneous dielectric/magnetic material. *Progress In Electromagnetics Research*, Vol.60:pages 49–62, 2014.

[16] E. A. Soliman A. A. Sakr and A. K. Abdelmageed. Electromagnetic TE scattering by a conducting cylinder coated with an inhomogeneous dielectric/magnetic material. *Journal of Electromagnetic Waves and Applications*, pages 1376–1387, 2014.

[17] E. Koné. *Équations intégrales volumiques pour la diffraction d'ondes électromagnétiques par un corps diélectrique.* PhD thesis, UNIVERSITÉ DE RENNES 1, 2010.

[18] C. Daveau A. Aubakirov and P. Soudais. High order impedance boundary condition for mom scattering. *IEEE Antennas and Propagation*, 2013.

[19] M. Fares A. Bendali and J. Gay. A boundary-element solution of the leontovich problem. *IEEE Trans. Antennas Propagat.*, Vol. 47:pages 1597–1605, October 1999.

[20] A. W. Glisson. An integral equation for electromagnetic scattering from homogeneous dielectric bodies. *IEEE Trans. Antennas Propag.*, 1984.

[21] A. Menshov and V. Okhmatovski. New single-source surface integral equations for scattering on penetrable cylinders and current flow modeling in 2-d conductors. *IEEE Trans. Microwave Theory Tech.*, 2013.

[22] A. J. Poggio and E. K. Miller. Integral equation solutions of three-dimensional scattering problems. *Computer Techniques for Electromagnetics, Chap. 4*, 1973.

[23] G. Nakamura H. Wang. The integral equation method for electromagnetic scattering problem at oblique incidence. *ELSEVIER*, Vol.62(No 4):pages 860–873, April 2012.

[24] M. Naser-Moghadasi S. Hatamzadeh-Varmazyar. An integral equation modeling of electromagnetic scattering from the surfaces of arbitrary resistance distribution. *Progress In Electromagnetics Research*, Vol.B(No 3):pages 157–172, 2008.

[25] L. Nicolas T. Jacques and C. Vollaire. Implementation of the boundary integral method for electromagnetic scattering problems with geometrical discontinuities. *IEEE TRANSACTIONS ON MAGNETICS*, Vol.38(No 2):pages 753–756, March 2002.

[26] Roger F. Harrington. *Time-Harmonic Electromagnetic Fields*. Wiley, 2001.

[27] M. A. Leontovich. Investigation of propagation of radiowaves. *Acad. Sci*, pt(II), 1948.

[28] Y. Rahmat-Samii and J.H Daniel. *Impedance boundary conditions in electromagnetics*. Taylor & Francis, 1995.

[29] T.B.A. Senior and J.L. Volakis. Approximate boundary conditions in electromagnetics. *IEE Electromagnetic Waves Series*, 41, 1995.

[30] A. W. Glisson. Electromagnetic scattering by arbitrary shapes surfaces with impedance boundary conditions. *Radio Sci.*, Vol. 27(No. 6):pages 935–943, May 1992.

[31] S. Sharma. An accelerated surface integral equation method for the electromagnetic modeling of dielectric and lossy objects of arbitrary conductivity. *IEEE Transactions on Antennas and Propagation*, 2021.

[32] M. Cessenat. *Mathematical Methods in Electromagnetism - Linear Theory and Applications*. Series on advances in Mathematics for applied science, 2016.

[33] N. Chaulet. *Modèles d'impédance généralisée en diffraction inverse*. PhD thesis, École de Polytechnique Paris, 2012.

[34] B. Stupfel and Y. Pion. Impedance boundary conditions for finite planar or curved frequency selective surfaces. *IEEE Trans. Antennas Propagat.*, Vol. 53:pages 1415–1424, April 2005.

[35] G. C. Hsiao and R. F. Kleinman. Mathematical foundations for error estimations in numerical solutions of integral equations in electromagnetics. *IEEE Trans. Antennas Propagat*, 45: 316–328, March (1997).

[36] J. G. Van Bladel. *Electromagnetic Fields*. 2nd edition, 2007.

[37] G. C. Hsiao and R. F. Kleinman. foundations for error estimations in numerical solutions of integral equations in electromagnetics. *IEEE Trans. Antennas Propagat.*, 45:pages 316–328, 1997.

[38] D. Drivaliaris and N. Yannakakis. Generalizations of the lax-milgram theorem. *arXiv*, V1, 2008.

[39] V. Lange. *Equations intégrales espace-temps pour les équations de Maxwell: calcul du champ diffracté par un obstacle dissipatif*. PhD thesis, Bordeaux, 1995.